Molecular Therapy
Oncolytics
Original Article

A Novel Antitumor Strategy: Simultaneously Inhibiting Angiogenesis and Complement by Targeting VEGFA/PIGF and C3b/C4b

Huiling Wang,[1,4] Yiming Li,[1,3,4] Gang Shi,[1,4] Yuan Wang,[1] Yi Lin,[1] Qin Wang,[1] Yujing Zhang,[1] Qianmei Yang,[1] Lei Dai,[1] Lin Cheng,[1] Xiaolan Su,[1] Yang Yang,[1] Shuang Zhang,[2] Zhi Li,[3] Jia Li,[3] Yuquan Wei,[1,2] Dechao Yu,[1,2] and Hongxin Deng[1]

[1]State Key Laboratory of Biotherapy and Cancer Center/Collaborative Innovation Center of Biotherapy, West China Hospital, Sichuan University, Chengdu, Sichuan 610041, P.R. China; [2]Department of Biotherapy, Cancer Center, West China Hospital, Sichuan University, Chengdu, Sichuan 610041, P.R. China; [3]Innovent Biologics (Suzhou) Co., Ltd., Suzhou, Jiangsu 215000, China

Therapeutic antibodies targeting vascular endothelial growth factor (VEGF) have become a critical regimen for tumor therapy, but the efficacy of monotherapy is usually limited by drug resistance and multiple angiogenic mechanisms. Complement proteins are becoming potential candidates for cancer-targeted therapy based on their role in promoting cancer progression and angiogenesis. However, the antitumor abilities of simultaneous VEGF and complement blockade were unknown. We generated a humanized soluble VEGFR-Fc fusion protein (VID) binding VEGFA/PIGF and a CR1-Fc fusion protein (CID) targeting C3b/C4b. Both VID and CID had good affinities to their ligands and showed effective bioactivities. *In vitro*, angiogenesis effects induced by VEGF and hemolysis induced by complement were inhibited by VID and CID, respectively. Further, VID and CID confer a synergetic therapeutic effect in a colitis-associated colorectal cancer (CAC) model and an orthotopic 4T1 breast cancer model. Mechanically, combination therapy inhibited tumor angiogenesis, cell proliferation, and MDSC infiltration in the tumor microenvironment and promoted tumor cell apoptosis. Our study offers a novel therapeutic strategy for anti-VEGF-resistant tumors and chronic-inflammation-associated tumors.

INTRODUCTION

Cancer is a major public health problem that causes death by increasing morbidity. However, progress has been made in only a few types of tumors. Most solid tumors still lack effective treatment.[1–3] In the early 1980s, Folkman put forward the view that "tumor growth depends on angiogenesis."[4] A number of anti-angiogenesis drugs, such as bevacizumab (Avastin), which inhibits the activity of vascular endothelial growth factor (VEGF), and multi-target anti-angiogenic drugs (sunitinib and sorafenib) have already been widely used with cancer patients.[4,5] However, an increasing number of cases of resistance to anti-angiogenesis therapy have emerged.[6–8] It has been reported that the withdrawal of bevacizumab accelerates tumor regrowth in patients with colorectal cancer[9,10] and that monotherapy of anti-VEGF antibody induces tumor hypoxia and potentiates the growth of human colon cancer xenografts.[11] In addition, studies have reported that inhibitors targeting the VEGF pathway concomitantly elicit tumor adaptation ability and then progress to a high malignant degree in mouse models of pancreatic neuroendocrine carcinoma and glioblastoma.[9] These findings raise the question of how to improve the efficacy of antitumor angiogenesis therapy.

Immune escape is a key factor in tumor development;[12–15] blocking tumor immune escape is an interesting strategy for tumor therapy. Complement acts as a first defense against microorganism invasion and widely participates in immune regulation, which plays an important role in the occurrence of inflammation, tumor development, and other diseases. In recent years, the relevance between complement system and cancer development has become a research focus. Complement activation can inhibit tumor cell apoptosis and promote tumor angiogenesis and immune escape,[16] making it a potential target for tumor therapy.

It has been reported that complement activation and C5a signaling are involved in the recruitment of myeloid-derived suppressor cells (MDSCs) into the tumor environment and the suppression of $CD8^+$ T cell-mediated tumor killing.[17] In addition, previous studies indicated that $CD31^+$ endothelial cells in angiogenesis were significantly impaired in both $C3^{KO}$ and C5aR (C5a receptor)^{KO} mice.[18] Further, tube formation of human umbilical vein endothelial cells (HUVECs) was shown to be C5a dependent, possibly through interactions with the VEGF165, but not the VEGF121, isoform.[19]

Received 28 May 2019; accepted 9 December 2019;
https://doi.org/10.1016/j.omto.2019.12.004.

[4]These authors contributed equally to this work.

Correspondence: Dechao Yu, Innovent Biologics (Suzhou) Co., Ltd., 168 Dongping Street, Suzhou, Jiangsu, 215000, P.R. China.
E-mail: michael.yu@innoventbio.com
Correspondence: Hongxin Deng, State Key Laboratory of Biotherapy and Cancer Center/Collaborative Innovation Center of Biotherapy, West China Hospital, Sichuan University, Ke-yuan Road 4, No. 1, Gao-peng Street, Chengdu, Sichuan, 610041, P.R. China.
E-mail: denghongx@scu.edu.cn

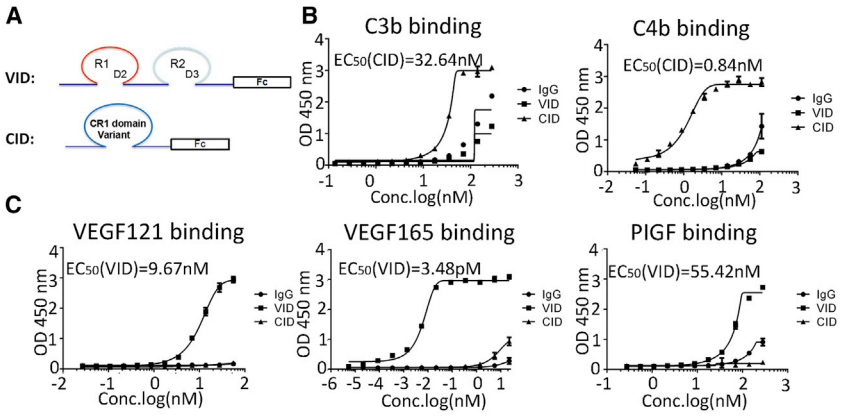

Figure 1. Molecular and Biochemical Characteristics of VID and CID

(A) Schematic diagram outlines the structure of VID and CID. (B) Comparison of binding affinity of CID, VID, and IgG to C3b and C4b as determined by ELISA. The average of triplicates is indicated with bars representing SD. OD_{450}, optical density 450. (C) Comparison of binding affinity of CID, VID, and IgG to VEGF121, VEGF165, and PlGF as determined by ELISA. The average of triplicates is indicated with bars representing SD.

The tumorigenesis, progression, and metastasis are complex processes involved with multiple mechanisms and pathways, which impose great challenges on the development of antibody drugs. The majority of these drugs only target a single target, leading to the limited outcomes. In order to improve the therapeutic effect and explore the multi-target combination therapy, we hypothesized that simultaneous inhibition of VEGF and complement component would exert a strong antitumor ability via inhibiting angiogenesis and releasing an immune response. To prove this hypothesis, we first generated a soluble VEGF inhibition domain (VID) blocking VEGF-A/PlGF (placental growth factor) and a soluble complement-inhibited domain (CID) blocking C3b/C4b in the complement activation process and then tested this strategy in a mouse colitis-associated colorectal cancer (CAC) model and in orthotopic breast cancer models. Our findings demonstrated that the combination therapy effectively inhibited tumor angiogenesis and released antitumor immunity, resulting in a significant tumor control. Our present data provide the theoretical and experimental evidence for multi-targeted combination treatment of cancer.

RESULTS

Characterization of VID and CID

The humanized soluble VID consists of the second immunoglobulin G (IgG)-like domain of VEGFR1, the third IgG-like domain of VEGFR2, and humanized Fc antibody fragments (Figure 1A). The humanized soluble CID has high binding affinity for C3b and C4b (Figure 1A). Both VID and CID form a stable dimer, and their molecular mass is 124 kDa and 106.4 kDa, respectively, which is verified by high-performance liquid chromatography-mass spectrometry (HPLC-MS) (Figures S1A–S1D). The detailed information of VID and CID is described in the Patent Cooperation Treat (PCT, patent no. WO2013082563 A1).

Binding Affinity of VID and CID

To evaluate the affinity activity of VID and CID with their ligands, ELISA assays were conducted, and results revealed that CID was able to bind complement proteins C3b and C4b, but not any of the VEGF-A isoforms, with the EC_{50} (the concentrations that result in half-maximal effect) at 32.64 nM (n = 3) and 0.84 nM (n = 3) (Figure 1B). VID could bind to human VEGF-A121, VEGF-A165, and PlGF, but not C3b or C4b, with the EC_{50} values at 9.67 nM (n = 3), 3.48 pM (n = 3), and 55.42 nM (N = 3), respectively (Figure 1C). Further, the competitive binding assays showed that VID blocked the biotinylated VEGF binding to the KDR (kinase insert domain receptor, also kown as VEGFR2), and that CID blocked biotinylated C4b binding to the CD35 (CR1) (Figure S2).

Thus, these data suggested that both CID and VID have specific binding capacities to their targets *in vitro*.

VID Inhibited the Proliferation, Migration, and Tube Formation of HUVECs *In Vitro*

In order to evaluate the bioactivity of VID, VEGF-induced HUVEC migration, tube formation, and proliferation assays were used. First, we observed that the proliferation of HUVECs was inhibited in the VID group ($p < 0.001$) and in combination treatment ($p < 0.005$) (Figure 2A); the addition of CID would not affect the inhibitory effect of VID on VEGF in the combined group. Furthermore, the tube formation assay proved that HUVECs treated with 10 ng/mL VEGF showed more tube-like structures than cells in basal medium ($p < 0.001$). However, VEGF-induced tube formation was significantly inhibited by VID ($p < 0.001$). Additionally, the number of branch structures also decreased significantly when VID and CID were administrated simultaneously (combined group [VID+CID]; $p < 0.001$) (Figures 2B and 2C). The capacity of VID and combination treatment to inhibit HUVEC migration was investigated with a Transwell chamber assay. Similarly, a significant increase of migrated cells was observed in the VEGF-A165 group (10 ng/mL) compared to that in the untreated group ($p < 0.001$). When VID was added into VEGF-containing medium, the number of migrating cells was significantly reduced, compared with that in the VEGF-treated group ($p < 0.001$). The combined group had the same decrease in migration as the VID group ($p < 0.001$) (Figures 2D and 2E). The aforementioned results indicated VID had good biological activity *in vitro*.

CID Inhibited Complement Activation and Bioactivity of HUVECs *In Vitro*

To investigate the biological activity of CID, we examined the inhibitory effect of CID via classic pathway complement-mediated hemolysis (CH50) assays and alternative pathway complement-mediated

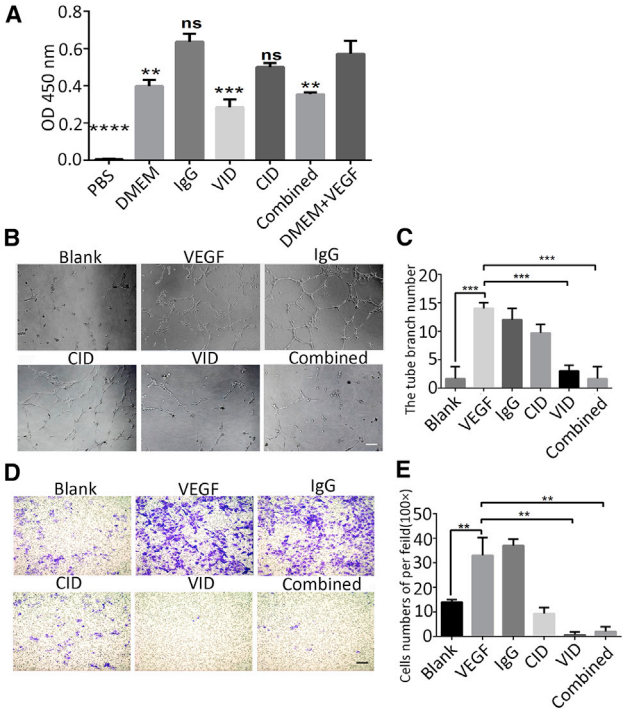

Figure 2. Bioactivity of VID *In Vitro*

(A) Comparison of HUVEC proliferation rate detected by CCK-8, with error bars representing SD. OD_{450}, optical density 450. (B) Endothelial tube formation was estimated following the incubation of HUVECs with conditioned media. 40×; scale bar, 200 μm. (C) The number of branches was quantified, with error bars representing SD. (D) HUVEC migration was estimated following the incubation with conditioned media. 100×; scale bar, 100 μm. (E) Cell migration rate was quantified, with error bars representing SD. **p < 0.005; ***p < 0.001; ****p < 0.0001; ns, not significant.

hemolysis (ACH50) assays (Figures 3A and 3B). Both results showed a decreasing trend in the percentage of the red blood cell hemolysis caused by human serum complement with increasing CID concentrations. Furthermore, we found that C5a receptor I, also called CD88, was highly expressed in HUVECs (Figure 3C), which indicated that C5a may be involved in the function of HUVECs. Therefore, we tested the inhibition ability of CID on HUVEC migration and tube formation induced by human serum complement. The results showed that CID could inhibit HUVEC migration and tube formation induced by complement sera ($p < 0.001$). Similar results were observed in the combined group ($p < 0.001$) (Figures 3D–3G). The addition of VID would not affect the inhibitory effect of CID on complement in the combined group. These results proved that CID had good biological activity *in vitro*.

Combination of CID and VID Could Effectively Inhibit the Occurrence of CAC in Mice

We have demonstrated that CID and VID could exert good bioactivity and strong binding affinities to their targeting proteins *in vitro*. Next, we established a mouse CAC model by administration of azoxymethane (AOM) followed by a dextran sodium sulfate (DSS) feed to investigate the therapeutic effect of combining CID and VID (Figure 4A). A histopathological review of the colon revealed chronic inflammation and epithelial damage by the repeated administration of DSS, resulting in epithelial hyperplasia and adenoma formation (Figure S3A). Since both VID and CID are humanized fusion proteins, we initially detected the affinity of VID to mouse VEGF164 (mVEGF164) and the inhibiting hemolysis effect of CID on mouse serum complement; the results demonstrated that both VID and CID have affinities to mouse targets (Figures S3B and S3C). In addition, the increasing expression of VEGF was observed in colonic mucosa during the process of CAC (Figure 4B). According to the activation process of the complement cascade, CID inhibits C5a in the tumor microenvironment by binding to C3b and C4b. Intriguingly, C5a expression increased from day 0 to day 45 and decreased at day 70 (Figure 4C). Decreased C5a level might be due to the internalization of the C5a/C5aR complex.

Next, we evaluated the effects of combining VID and CID on tumor growth and angiogenesis in the CAC model. Results revealed that there was no difference in tumor number among the control groups (PBS group or IgG group) or monotherapy (VID group or CID group). However, the average tumor number was significantly decreased in the combined group compared to the control groups (PBS group or IgG group) (Figure 4D). We classified the tumors into three levels by volume size: small (≤ 5 mm^3), medium (5–20 mm^3), and large (20–50 mm^3). Although there were no statistically significant differences in tumor number in each group with different sizes, the tumor distribution in the combined group was smaller than that in other groups (Figure S3D). In addition, there was no significant difference in the body weight of each group (Figure S4). PBS- or IgG-treated mice had obvious intestinal disorganization with swollen glands, and some areas showed tumor-like proliferative lesions, while the colorectal structure of the combined group remained normal and the colorectal structure of the VID or CID group remained relatively intact (Figure 4E). These results have proved remarkable tumor-control abilities of combining VID and CID in the CAC model.

To explore the mechanism of combination therapy of VID and CID, we examined cell proliferation by detecting proliferating cell nuclear antigen (PCNA), compared to the other four groups; results showed that decreased PCNA-positive cells were observed in mice receiving combination treatment (Figure 4E), and the result was further confirmed by the detection of PCNA expression (Figures 4E and 4F). Tumor angiogenesis is an important criterion for the development of tumors.[20] We analyzed vessel densities by CD31 immunofluorescence staining. In comparison with PBS treatment, blood vessel densities reduced in the combined group and in the VID group within intratumoral regions. Although no statistical significance was observed between the combined and VID groups, the latter showed a more swollen phenotype than the former in colonic structures (Figures 4E and 4G). These results demonstrated that combination treatment of VID and CID could suppress angiogenesis and cell proliferation, leading to a decreased tumor growth.

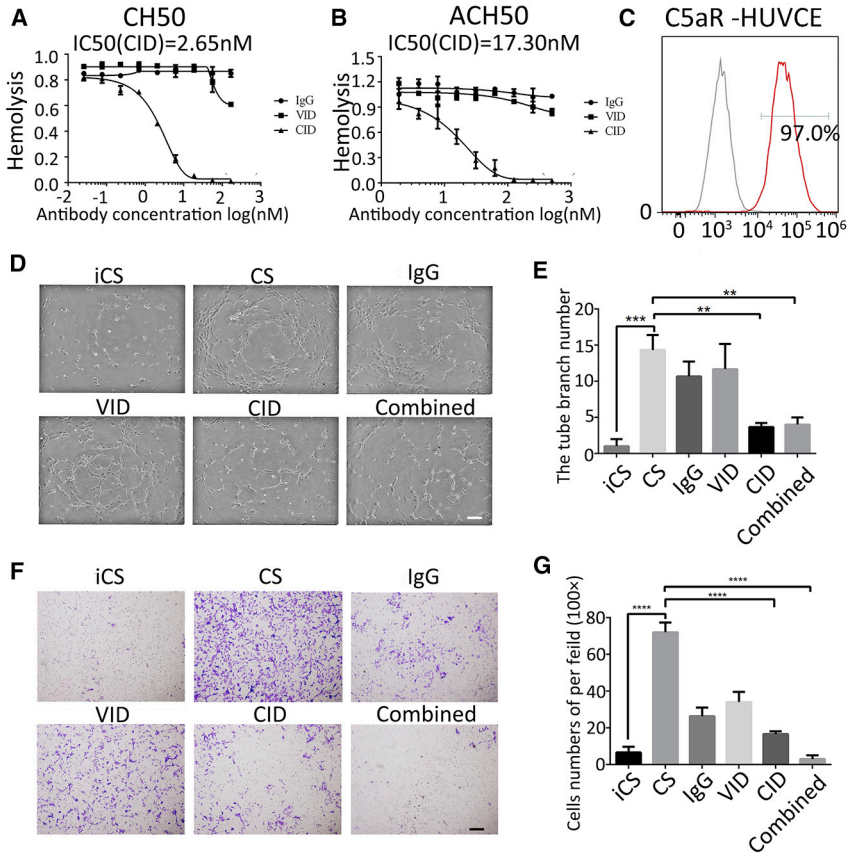

Figure 3. Bioactivity of CID *In Vitro*

(A) CID inhibits the activation of CH50. The average of triplicates is indicated, with bars representing SD. (B) CID inhibits the activation of ACH50. The average of triplicates is indicated, with bars representing SD. (C) Positive rate of C5aR in HUVECs by flow cytometry. (D) Endothelial tube formation was estimated following the incubation of HUVECs with conditioned media. 40×; scale bar = 200 μm. (E) The number of branches was quantified, with error bars representing SD. (F) HUVEC migration was estimated following the incubation with conditioned media. 40×; scale bar = 200 μm. (G) Cell migration rate was quantified, with error bars representing SD. ***$p < 0.001$; ****$p < 0.0001$.

Combination Treatment with VID and CID Suppressed MDSC Recruitment in Tumor Microenvironment

To further analyze the antitumor mechanism mediated by the combination therapy, we detected tumor-associated immune cells in the tumor microenvironment by flow cytometry. MDSCs that infiltrated into the colorectum were significantly inhibited after combination treatment, the percentage of infiltrated MDSCs in the combined group was almost consistent with that in normal mice (Figures 5A and 5B). This result was consistent with immunofluorescence staining (Figures 5C and 5D). However, no significant difference was observed in the percentage of T cells and macrophages (Figure S5). These results suggest that combination treatment can effectively inhibit tumor formation, possibly by inhibiting the recruitment of MDSCs in the microenvironment rather than other cells.

Combination Treatment with VID and CID Significantly Inhibited Mouse Orthotopic 4T1 Breast Cancer

To expand indications of combination treatment, we tested whether this treatment is effective in other models. First, we examined the expression of C3 and C5aR in mouse tumor cell lines, including 4T1, LL2, and CT26, except the low expressions of C3 in CT26, C3, and C5aR expression were detected in three tumor cell lines (Figure S6). We established an orthotopic 4T1 breast cancer model to further investigate the antitumor efficacy of combination treatment with VID and CID. Compared to the PBS group, tumor volume and weight were decreased in all treatment groups after treatment, especially in the combined group after 21 days of treatment (Figures 6A–6C). Mechanically, the combination treatment remarkably suppressed cell proliferation, which was determined via PCNA expression in tumor tissues; monotherapy with VID or CID also had inhibitory effects on tumor cell proliferation (Figures 6D and 6G). Furthermore, TUNEL assay results showed that, compared with the control groups (IgG and PBS), the combined group significantly promoted apoptosis of tumor cells (Figures 6E and 6H). Both VEGF and complement are related to angiogenesis, so we also analyzed tumor angiogenesis after treatment, in comparison with PBS treatment, and found that blood vessel densities were reduced in the combined group (Figures 6F and 6I). As 4T1 is a good tumor model for studying lung metastasis, we also determined the lung metastasis after treatment. Our results demonstrated that no apparent node metastasis was observed in the combination therapy group (Figure 6J; Figure S7). In addition, CID or VID monotherapy also restrained the number of node metastases (Figure 6J; Figure S7).

Our results suggested that combination treatment suppressed tumor growth and lung metastasis by inhibiting tumor angiogenesis and proliferation, increasing the apoptosis of tumor cells.

DISCUSSION

VEGF family members (mainly VEGF-A), as one of the most important factors for angiogenesis, have been widely regarded as a hallmark of cancer. Biological antitumor drugs targeting VEGF, such as bevacizumab, have achieved great success.[21] However, further studies remain to be explored in light of the fact that drug resistance has emerged.[22–25] Previous studies have found that VEGF Trap, compared with VEGF monoclonal antibody, has higher affinity, better pharmacokinetics, and a stronger inhibitory effect.[26] VID, as one type of the VEGF Trap, showed good biological activity in our *in vivo* and *in vitro* experiments. However, from our point of view, a single pathway is not enough to inhibit tumor angiogenesis.

Increasing evidence has shown that pro-angiogenic factors derived from tumor cells or induced after therapy in the tumor microenvironment could promote angiogenesis.[27] C5a, as a pro-angiogenic factor, promotes tube formation and cell migration of HUVECs *in vitro*, thus contributing to tumor angiogenesis.[28] In addition, C3a and C5a stimulate the angiogenesis of choroid vessels, a serious complication of age-related macular degeneration (AMD).[29] It has been reported that a novel bispecific molecule targeting VEGF and complement proteins delivered by recombinant adeno-associated virus 2 (AAV2) suppresses ocular inflammation and choroidal neovascularization.[30]

In our study, different stimulation that induces HUVEC tube formation and cell migration could be inhibited by VID and CID, which supports our hypothesis that angiogenesis could be regulated by different pathways. Thus, our results indicate that an anti-complement pathway could be a potential strategy for anti-angiogenesis treatment. In our study, the combination treatment with VID and CID does not show superior effects in biologic function assay *in vitro* (Figures 2A, 2C, 2E, 3D, and 3F). Inhibiting tumor angiogenesis may be attributed to different pathways on which VID and CID depend, since VID inhibited VEGF-induced angiogenesis effectively but not angiogenesis induced by complement. Similarly, CID inhibited the angiogenesis induced by complement but not angiogenesis induced by VEGF. These results clearly elucidated the different functions of VID and CID and also provided the evidence that tumor angiogenesis depends on different pathways.

An increasing number of studies have shown that the complement system also plays an important role in tumor progression.[31] Complement cascade activation causes anaphylatoxin C3a and C5a release. C3a and C5a are important inflammatory mediators and chemokines,[32] which are upregulated in patients with lung cancer, colorectal cancer, ovarian carcinoma, and cutaneous squamous cell carcinoma,[33–37] providing the feasibility of treating tumors through inhibiting complement activation. In our study, complement receptor 1 was the functional domain of CID, which could bind naturally to C3b and C4b, and it could effectively block complement cascade activation and inhibit C5a completely and C3a partially.[38]

Differing from acute inflammation, chronic inflammation contributes to tumorigenesis.[39,40] The AOM/DSS-induced CAC model has sustained inflammation, which realistically mimics the process of colorectal cancer in human.[41] The activation of the complement system may lead to chronic inflammation and boost the immunosuppressive tumor microenvironment by recruiting immune-suppressive cells.[42,43] Our results proved that C5a production was decreased from day 45 (Figure 4C) and that MDSC infiltration was significantly inhibited after combination therapy. This is consistent with findings from previous studies that C5a could attract immune-suppressive cells.[17,43]

It was reported that VEGF could promote immune escape through recruiting MDSCs into ovarian cancer.[44] In our study, however, VID alone did not show obvious anti-tumor effects or inhibit MDSC infiltration. Preclinical studies raised the possibility that VEGF inhibitors could suppress tumor growth but also promote tumor escape.[45] In addition, MDSCs promoted tumor formation in lung cancer and colorectal cancer via a VEGF-independent pathway.[11,46,47] Due to the dose of VID and CID being halved, the results of vessel density (Figure 4G) and MDSC infiltration (Figure 5B) in the combined group showed no particular superiority to individual treatment. We speculated that a proper increase in dosage may lead to better results.

Complement has been linked to metastasis in recent studies.[48] Report showed that stimulation of C5aR1 via C5a could induce an epithelial-to-mesenchymal transition (EMT), which was linked to ERK1/2 signaling in hepatocellular carcinoma.[49] C5a has been reported to promote breast cancer lung metastasis by defining the polarization of Th0 cells, recruiting MDSCs, and inducing angiogenesis.[19,50] We found that C5aR was highly expressed in 4T1 cells, and we established that a 4T1 orthotopic model, in which breast tumors formed *in situ* and subsequently metastasized to distant sites, was similar to human malignancy.[51] In the results, the combination therapy has valid antitumor effects compared to VID or CID alone. Considering that breast cancer is a malignant disease with a high recurrence or metastasis rate, our combination treatment showed effective tumor control and inhibition of lung metastasis, suggesting a potential strategy for breast cancer therapy in clinic.

Overall, we generated humanized soluble VID targeting VEGFA/PIGF and CID targeting C3b/C4b. These two fusion proteins have good affinities and biological activities both *in vitro* and *in vivo*. We established that the combination therapy with VID and CID shows effective tumor inhibition in the mouse CAC model and orthotopic 4T1 tumor. Our present results also show two independent pathways to inhibit tumor angiogenesis by separately blocking VEGF and complement. Moreover, CID could effectively block complement cascade activation and inhibit C5a to reduce the infiltration of MDSCs in the tumor microenvironment. We hope that this study will provide novel theoretical and experimental evidence for multi-targeted treatment of tumors.

MATERIALS AND METHODS

Generation of VID and CID

To generate humanized soluble VID, we fused the second IgG-like domain of VEGFR1, the third IgG-like domain of VEGFR2, and humanized Fc antibody fragments and removed positive charges associated with the extracellular matrix. Meanwhile, the first three domains of soluble complement receptor 1(sCR1) were replaced using N29K, S37Y, G79D, and D109N amino-acid substitutions to enhance its binding affinity to C3b and C4b and then were fused with the Fc region of human immunoglobulin to generate CID. The detailed information of VID and CID was described in the PCT patent (patent no. WO2013082563 A1). Recombinant proteins were expressed by a CHO-E system to obtain high

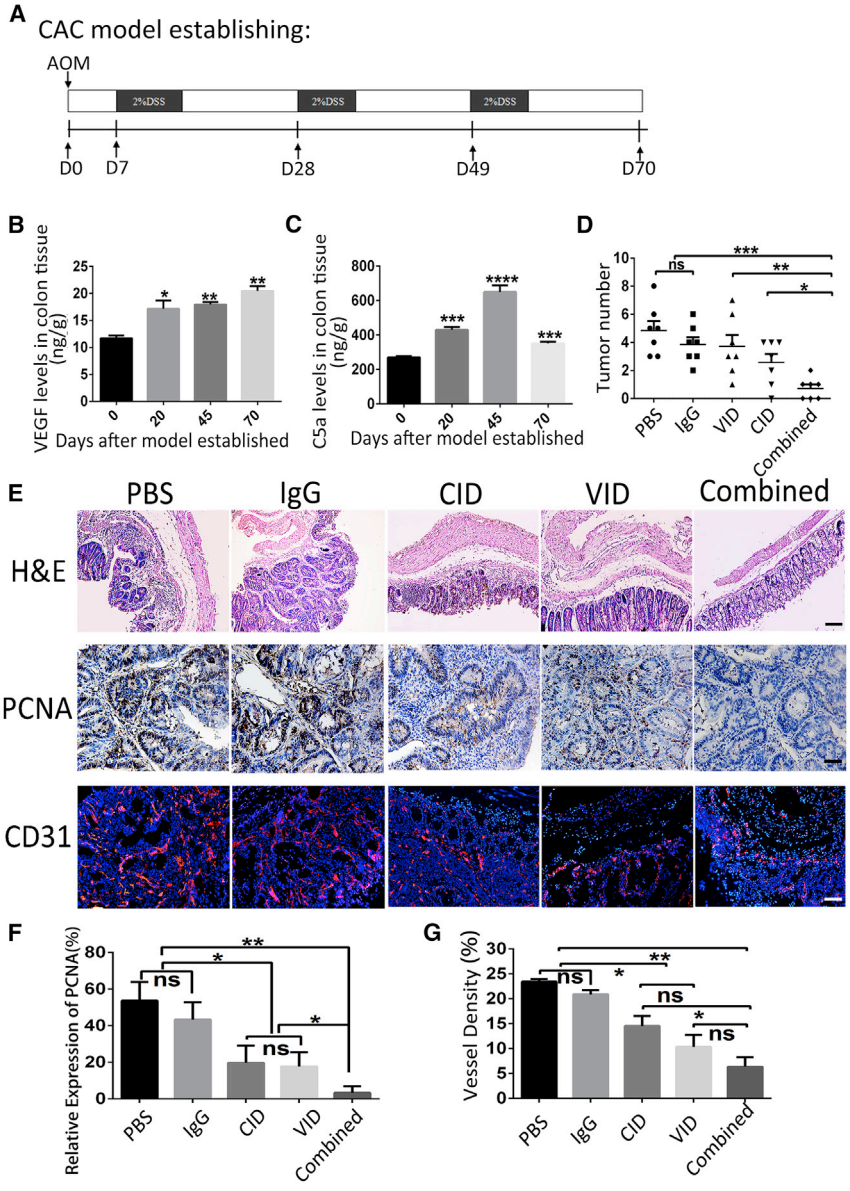

Figure 4. Combination of VID and CID Reduces CAC Tumorigenesis

(A) Schematic overview of CAC regimen. (B and C) At the indicated time points after initiation of CAC induction, colons were homogenized, and supernatants were prepared for the detection of VEGF (B) and C5a (C) protein levels. Each group consisted of 3–4 mice. The error bars represent SD (***p < 0.001; ****p < 0.0001; *versus day 0, all groups are compared to D0). (D) Number of tumors in colon and rectum was counted, with bars representing SD. ns, not significant. (E) H&E, PCNA, and CD31 staining of the colon of mice. For H&E staining: original magnifications, 100×. Scale bars, 100 μm. (F) Representative immunohistochemistry images with antibody to PCNA in different groups; original magnifications, 200×; and quantification analyses of PCNA-positive cell number, with error bars representing SD (*p < 0.01; **p < 0.005; ns, not significant). (G) Immunofluorescence analysis using anti-CD31 (red) antibody indicates the blood vessel outlines of different groups. The error bars represent SD (*p < 0.01; **p < 0.005; ns, not significant). 100×; scale bar, 100 μm.

expression levels, and recombinant protein was purified by affinity chromatography.

Binding Assay

The binding ability and affinity of VID, CID, or IgG to VEGF-A165, VEGF-A121, PIGF, C3b, or C4b were measured by enzyme-linked immunosorbent assay (ELISA). VEGF-A165, VEGF-A121, PIGF, and IgG were purchased from PeproTech. C3b and C4b were purchased from Millipore. Briefly, 50 ng VEGF-A165, VEGF-A121, and PIGF and 250 ng C3b and C4b in 100 μL PBS were added into 96-well plates and incubated at 4°C overnight. After washing the plate three times with 300 μL PBS, the plates were incubated with blocking solution (1% BSA in 100 μL phosphate-buffered saline [PBS]) at 37°C for 2 h. Serially increasing amounts (0.05–50 nM) of VID or CID in 100 μL blocking solution were added to the plate and incubated at 37°C for 2 h. IgG served as the negative control. After a series of reactions, the reactive colors were analyzed at an optical density of 450 nm (OD_{450}) using a microplate reader (MK3, Thermo Fisher Scientific, Waltham, MA, USA)

Cell Culture

HUVECs were maintained in EndoGRO-VEGF medium (Millipore, Burlington, MA, USA) at 37°C, in a 5% CO_2 humidified incubator. Mouse 4T1 breast tumor cells were maintained in RPMI 1640 (GIBCO, Waltham, MA, USA) containing 10% fetal bovine serum (FBS; GIBCO) and grown at 37°C in 5% CO_2. Both of the cell lines were obtained from the American Type Culture Collection (ATCC, Rockville, MD, USA). All culture media were supplemented with 100 U/mL penicillin, 100 μg/mL streptomycin. Cell line authentication was assessed using a short tandem repeat DNA profiling method in our laboratory, and the latest verification was done in July 2013. The mycoplasma detecting kit (catalog no. MD001), purchased from Shanghai Yise Medical Technology was performed to test whether there were mycoplasma contamination.

Biological Activity of VID and CID *In Vitro*

HUVEC Migration Assay

8×10^4 cells were cultured in 24-well plates in EndoGRO-basic medium on the upper chamber of Transwells with an 8-mm pore size (Corning-Costar, Corning, NY, USA). 10 ng/mL VEGF

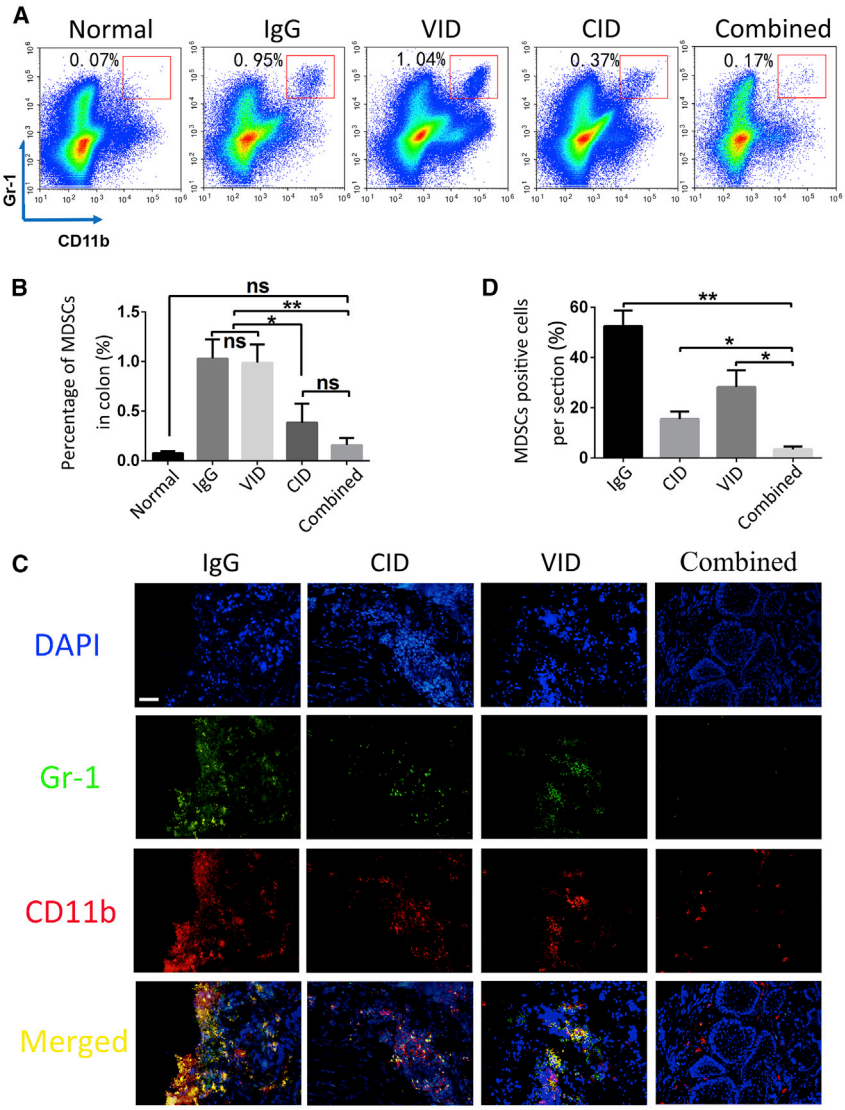

Figure 5. Infiltration of MDSCs in Colon

(A and B) Infiltration of MDSCs in colon was analyzed by flow cytometry (A) and quantification analyses of MDSC ($Gr\text{-}1^+CD11b^+$-positive cell) numbers in colon (B). Each bar represents the mean with SD (**$p < 0.005$; ***$p < 0.001$; ns, not significant). (C) Immunofluorescence analysis using anti-CD11b (red) antibody and anti-Gr-1 (green) antibody co-located in MDSCs in colons of different groups. Original magnification, 100×; scale bar = 100 μm. (D) Quantification analyses of MDSCs ($Gr\text{-}1^+CD11b^+$-positive cell) numbers in colon, with error bars representing SD (*$p < 0.01$; ***$p < 0.005$).

or 20 μL Human Serum Complement (Sigma-Aldrich, St. Louis, MO, USA) was added respectively. IgG, VID, CID, and VID+CID at the concentration 35 nmol/L were added in different wells. EndoGRO-basic and EndoGRO-VEGF media were used as negative and positive controls. After a 24-h incubation, cells from the upper chambers were removed, and cells adhered to the lower side of Transwells were fixed with 4% formaldehyde and stained with 0.5% crystal violet. Migrated cells on the lower surface of the filter were photographed using an Olympus BX600 microscope and SPOT Flex camera. At least three fields at 100× magnification were taken and counted using ImageJ software.

Tube Formation Assay

2×10^4 HUVECs were plated in 2 mL DMEM (GIBCO, Waltham, MA, USA) containing 10% FBS. Conditioned medium was collected 48 h later. The wells of a 96-well plate were coated with ice-chilled BD Matrigel matrix gel solution (BD Biosciences, San Jose, CA, USA). 2×10^4 HUVECs were plated in 100 μL conditioned medium with VEGF (10 ng/mL) or human serum complement (20 μL) and antibodies (IgG, VID, CID or VID+CID) at a concentration of 35 nmol/L. Cells were incubated for 4 h at 37°C and were visualized by light microscopy. The degree of angiogenesis was quantified by counting the number of cells in branch point capillaries (≥3 cells per branch) in three random fields per replicate.

HUVEC Proliferation Assay

2×10^3 HUVECs were seeded into 96-well plates with EndoGRO-VEGF medium and replaced by DMEM containing 10 ng/mL VEGF after 24 h. Then, 35 nM IgG, VID, or CID or 17.5 nM VID+CID was added respectively; DMEM as negative control, a positive control for DMEM with VEGF, a blank control with only PBS were set. Each group was set up with three repetitions. After 48 h, 10 μL Cell Counting Kit-8 (CCK-8) solution was added into each hole and detected them with a microplate reader at 450 nm.

CH50 Assay

50 μL human complement serum was added into a 96-well plate. Different diluted antibodies (IgG, VID, CID or VID+CID) were added. Then, samples were mixed with immunized 1×10^8 sheep red blood cells in conditional gelatin veronal buffer-EDTA buffer (GVB-EDTA buffer; 0.1% gelatin, 5 mM barbitone, 145 mM NaCl, 10 mM EDTA). GVB-EDTA buffer and deionized water were used as negative and blank controls, respectively. Samples were placed in a shaker at 37°C at 130 rpm for 45 min, followed by centrifugation at 1,000 × *g*, at 15°C for 3 min. Each group was set up with three repetitions. 100 μL supernatant was collected in 96-well plates and detected at OD_{405} with a microplate reader.

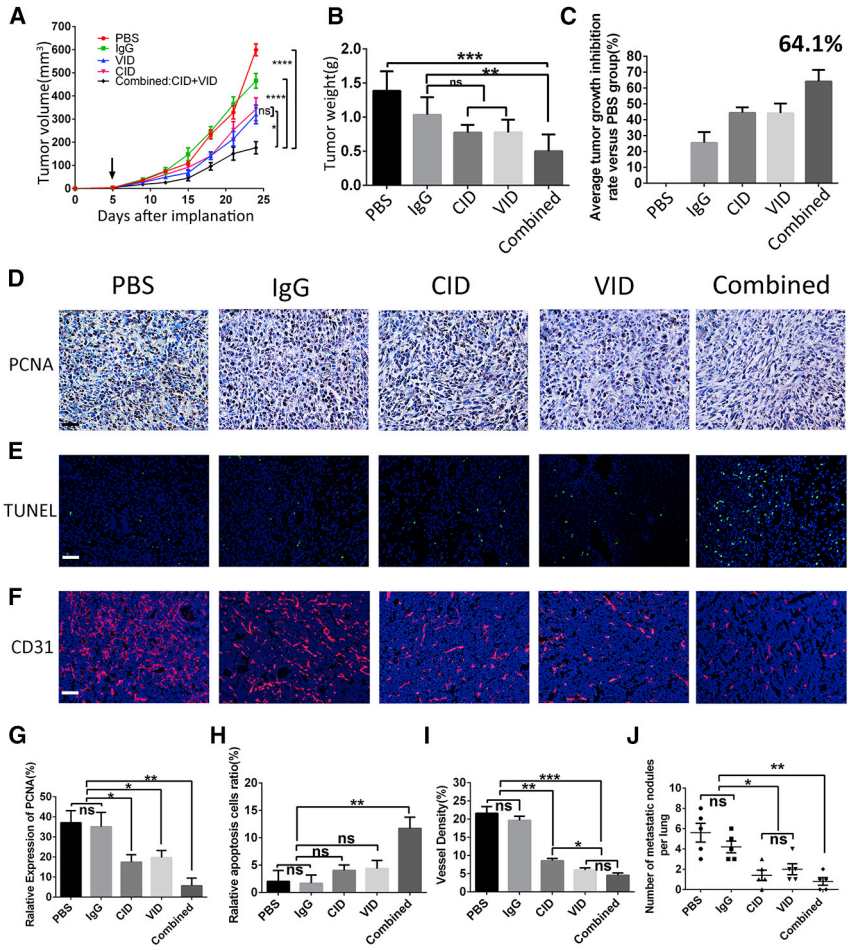

Figure 6. Combination of VID and CID Suppresses Tumor Growth in Breast-Tumor-Bearing Mice

(A) Comparison of tumor growth; arrow indicates the start of injections. Error bars represent SD (*p < 0.01; ****p < 0.0001; ns, not significant). (B) Tumor weight of mice in each group was measured on the days indicated, with error bars representing SD. (C) Results of tumor inhibition rate in each experimental group. (D–I) In (D) and (G), representative immunohistochemistry images (D) are shown with antibody to PCNA in different groups (original magnifications, 200×; scale bar, 50 μm) and quantification analyses (G) of PCNA positive-cell number are presented, with error bars representing SD (*p < 0.01; **p < 0.005; ns, not significant). (E and H) Detection of apoptosis of tumor cells by TUNEL (E) (200×; scale bar, 50 μm) and quantification analyses of TUNEL-positive cell numbers (H), with error bars representing SD (**p < 0.005; ns, not significant). (F and I) Immunofluorescence analysis (F) using anti-CD31 (red) antibody shows blood vessel outlines of different groups; in quantification analyses (I), error bars represent SD (*p < 0.01; **p < 0.005; ***p < 0.005; ns, not significant; 100×; scale bar, 100 μm). (J) Quantification of lung metastasis nodule of 4T1 cells in different groups, with error bars representing SD (*p < 0.01; **p < 0.005; ns, not significant).

ACH50 Assay

20 μL human complement serum was added into each 96-well plate. Different diluted antibodies (IgG, VID, CID, or VID+CID) were added. Then, 10 μL, 0.16 mM Mg^{2+} EDTA buffer was added into each well. GVB-EDTA buffer and deionized water were used as negative and blank controls. The conditional GVB-EDTA buffer with 2.5×10^8 rabbit red blood cells was added and then placed in a shaker at 37°C at 130 rpm for 45 min, followed by centrifugation at 1,000 × *g* at 15°C for 3 min. Each group was set up with three repetitions. 100 μL supernatant was collected in 96-well plates and detected at 405 nm with a microplate reader.

$$\text{Hemolysis rate} = (\text{experimental group} - \text{blank control group})/ \times (\text{negative} - \text{blank control group})$$

Generation of Tumor Models and Treatment Regimes

6- to 7-week-old male C57BL/6J mice were used in the CAC model for pharmacodynamic evaluation. Mice were randomly divided into 5 groups, and each group included 5 mice. Mice were injected intraperitoneally with AOM (10 mg/ kg) on day 1, were maintained on a regular diet and water for 7 days, and then received water with 2% DSS for 1 week. After this, mice were maintained on regular water for 2 weeks and subjected to two more DSS treatment cycles. According to the expression of VEGF and C5a in the development of CAC, mice were treated at a dose of 15 mg/kg VID, CID, IgG, and a combination of CID and VID (7.5 mg/kg each) on days 1, 3, and 5 of every cycle of DSS consumption. PBS gourp was used as negtive control.

In the 4T1 orthotopic breast cancer model, 6- to 7-week-old virgin female BALB/c mice were inoculated with 6×10^4 4T1 cells in the fourth right mammary fat pad. The mice were randomly divided into five groups, and each group included 6 mice. The therapeutic regime last 3 weeks, starting at the fourth day after 4T1 cells inoculation; mice were treated at a dose of 15 mg/kg VID, CID, IgG, or a combination of CID and VID (7.5 mg/kg each) three times a week. PBS gourp was used as negtive control. Tumor size was measured twice a week. The tumor volumes were calculated based on the modified ellipsoidal formula: tumor volume = (length × width^2) × 0.5. Animal studies were carried out in accordance with the West China Hospital Sichuan University Division of Comparative Medicine guidelines for the care and use of laboratory animals.

Immunofluorescence Staining

Frozen cryosections of colon tissue and tumors from mice were fixed in chilled acetone for 15 min before staining. Antibodies targeting different cell markers were as follows: CD31 (Abcam, London,

England), CD11b (Abcam), Gr-1 (BioLegend, San Diego, CA, USA). Secondary antibodies were labeled with FITC-Texas Red (Santa Cruz Biotechnology, Santa Cruz, CA, USA), while the nuclei were detected by DAPI (Roche, Basel, Switzerland). All specimens were evaluated using an Olympus BX600 microscope and a SPOT Flex camera.

DeadEnd TUNEL Assay

Tumor tissues were fixed by formalin and embedded in paraffin, and the blocks were cut into slices, followed by steps according to the instructions of The DeadEnd Fluorometric TUNEL System Kit (Promega, Madison, WI, USA).

Immunohistochemistry

Paraffin sections were blocked with Dual Endogenous Blocking Reagent and 20% normal rabbit serum (ZSGB-Bio, Beijing, China) and incubated with monoclonal rabbit anti-mouse PCNA antibodies (Proteintech, Beijing, China) overnight at 4°C, followed by incubation with a biotinylated goat anti-rabbit secondary antibody (ZSGB-Bio, Beijing, China). Quantification of immunoreactive cells was performed with NIS-Elements imaging software (Nikon, Tokyo, Japan).

Flow Cytometry

Fluorochrome-conjugated mouse FITC-CD45 (30-F11), PE-CD11b (M1/70), and APC/Cy7-Gr-1 (RB6-8C5) were purchased from BD Biosciences (Franklin Lakes, NJ, USA). For fluorescence-activated cell sorting (FACS), single-cell suspensions were blocked with CD16-CD32 antibodies (2.4G2; BD PharMingen). Surface staining for T cells and MDSC populations were performed with respective antibodies for 30 min at 4°C. MDSCs were identified as $CD11b^+$ $Gr\text{-}1^+$ cells.

Statistics

Statistical analyses were performed utilizing GraphPad software Prism v.6.0. Values are presented as mean ± SD. The p values were calculated using Student's t test or one-way analysis of variance (ANOVA). A p value of < 0.05 was considered as statistically significant.

SUPPLEMENTAL INFORMATION

Supplemental Information can be found online at https://doi.org/10.1016/j.omto.2019.12.004.

AUTHOR CONTRIBUTIONS

H.W., Y. Li, and G.S. were involved in acquisition of the data. H.D. was involved in the study concept and design. D.Y. was involved in obtaining funding. H.W. Y. Li and G.S. were involved in analysis and interpretation of the data, drafting of the manuscript, and critical revision of the manuscript for important intellectual content. Y. Lin and Y.Wang. were involved in the animal study. Q.W., Y.Z., and Q.Y. were involved in technical support for the binding and biological activity assay. L.D. and L.C. were involved in the technical support and analysis. X.S. and S.Z. participated in cell culture. Z.L. and J.L. helped to construct and prepare the fusion proteins. Y.Y. and Y.Wei. provided suggestions regarding the manuscript. H.D. supervised the whole experimental work and revised the manuscript. All authors read and approved the manuscript.

CONFLICTS OF INTEREST

The authors declare no competing interests.

ACKNOWLEDGMENTS

We thank Andy Tsun for article revision and Zhangyi Huang for assistance with statistical analysis. This work was supported by the National Natural Science Foundation of China (81372445).

REFERENCES

1. Bhatt, A.P., Redinbo, M.R., and Bultman, S.J. (2017). The role of the microbiome in cancer development and therapy. CA Cancer J. Clin. *67*, 326–344.
2. Chen, W., Zheng, R., Baade, P.D., Zhang, S., Zeng, H., Bray, F., Jemal, A., Yu, X.Q., and He, J. (2016). Cancer statistics in China, 2015. CA Cancer J. Clin. *66*, 115–132.
3. Heinemann, V., and Hoff, P.M. (2010). Bevacizumab plus irinotecan-based regimens in the treatment of metastatic colorectal cancer. Oncology *79*, 118–128.
4. Folkman, J. (2007). Angiogenesis: an organizing principle for drug discovery? Nat. Rev. Drug Discov. *6*, 273–286.
5. Ivy, S.P., Wick, J.Y., and Kaufman, B.M. (2009). An overview of small-molecule inhibitors of VEGFR signaling. Nat. Rev. Clin. Oncol. *6*, 569–579.
6. Casanovas, O., Hicklin, D.J., Bergers, G., and Hanahan, D. (2005). Drug resistance by evasion of antiangiogenic targeting of VEGF signaling in late-stage pancreatic islet tumors. Cancer Cell *8*, 299–309.
7. Pàez-Ribes, M., Allen, E., Hudock, J., Takeda, T., Okuyama, H., Viñals, F., Inoue, M., Bergers, G., Hanahan, D., and Casanovas, O. (2009). Antiangiogenic therapy elicits malignant progression of tumors to increased local invasion and distant metastasis. Cancer Cell *15*, 220–231.
8. Conley, S.J., Gheordunescu, E., Kakarala, P., Newman, B., Korkaya, H., Heath, A.N., Clouthier, S.G., and Wicha, M.S. (2012). Antiangiogenic agents increase breast cancer stem cells via the generation of tumor hypoxia. Proc. Natl. Acad. Sci. USA *109*, 2784–2789.
9. Cacheux, W., Boisserie, T., Staudacher, L., Vignaux, O., Dousset, B., Soubrane, O., Terris, B., Mateus, C., Chaussade, S., and Goldwasser, F. (2008). Reversible tumor growth acceleration following bevacizumab interruption in metastatic colorectal cancer patients scheduled for surgery. Ann. Oncol. *19*, 1659–1661.
10. Miles, D., Harbeck, N., Escudier, B., Hurwitz, H., Saltz, L., Van Cutsem, E., Cassidy, J., Mueller, B., and Sirzén, F. (2011). Disease course patterns after discontinuation of bevacizumab: pooled analysis of randomized phase III trials. J. Clin. Oncol. *29*, 83–88.
11. Miyazaki, S., Kikuchi, H., Iino, I., Uehara, T., Setoguchi, T., Fujita, T., Hiramatsu, Y., Ohta, M., Kamiya, K., Kitagawa, K., et al. (2014). Anti-VEGF antibody therapy induces tumor hypoxia and stanniocalcin 2 expression and potentiates growth of human colon cancer xenografts. Int. J. Cancer *135*, 295–307.
12. Hanahan, D., and Weinberg, R.A. (2011). Hallmarks of cancer: the next generation. Cell *144*, 646–674.
13. Hanahan, D., and Coussens, L.M. (2012). Accessories to the crime: functions of cells recruited to the tumor microenvironment. Cancer Cell *21*, 309–322.
14. Gajewski, T.F., Schreiber, H., and Fu, Y.X. (2013). Innate and adaptive immune cells in the tumor microenvironment. Nat. Immunol. *14*, 1014–1022.
15. Oleinika, K., Nibbs, R.J., Graham, G.J., and Fraser, A.R. (2013). Suppression, subversion and escape: the role of regulatory T cells in cancer progression. Clin. Exp. Immunol. *171*, 36–45.
16. Rutkowski, M.J., Sughrue, M.E., Kane, A.J., Mills, S.A., and Parsa, A.T. (2010). Cancer and the complement cascade. Mol. Cancer Res. *8*, 1453–1465.
17. Markiewski, M.M., DeAngelis, R.A., Benencia, F., Ricklin-Lichtsteiner, S.K., Koutoulaki, A., Gerard, C., Coukos, G., and Lambris, J.D. (2008). Modulation of the antitumor immune response by complement. Nat. Immunol. *9*, 1225–1235.

18. Nunez-Cruz, S., Gimotty, P.A., Guerra, M.W., Connolly, D.C., Wu, Y.-Q., DeAngelis, R.A., Lambris, J.D., Coukos, G., and Scholler, N. (2012). Genetic and pharmacologic inhibition of complement impairs endothelial cell function and ablates ovarian cancer neovascularization. Neoplasia *14*, 994–1004.

19. Vadrevu, S.K., Chintala, N.K., Sharma, S.K., Sharma, P., Cleveland, C., Riediger, L., Manne, S., Fairlie, D.P., Gorczyca, W., Almanza, O., et al. (2014). Complement c5a receptor facilitates cancer metastasis by altering T-cell responses in the metastatic niche. Cancer Res. *74*, 3454–3465.

20. Kerbel, R.S. (2008). Tumor angiogenesis. N. Engl. J. Med. *358*, 2039–2049.

21. Potente, M., Gerhardt, H., and Carmeliet, P. (2011). Basic and therapeutic aspects of angiogenesis. Cell *146*, 873–887.

22. Oumrani, S., Guillaumot, M.A., Brieau, B., Oudjit, A., Léandri, C., Brezault, C., Chaussade, S., and Coriat, R. (2017). Tumour growth increased following antiangiogenic interruption: the challenge of tumour evaluation. Anticancer Drugs *28*, 1062–1065.

23. Sennino, B., and McDonald, D.M. (2012). Controlling escape from angiogenesis inhibitors. Nat. Rev. Cancer *12*, 699–709.

24. Bottsford-Miller, J.N., Coleman, R.L., and Sood, A.K. (2012). Resistance and escape from antiangiogenesis therapy: clinical implications and future strategies. J. Clin. Oncol. *30*, 4026–4034.

25. Jayson, G.C., Kerbel, R., Ellis, L.M., and Harris, A.L. (2016). Antiangiogenic therapy in oncology: current status and future directions. Lancet *388*, 518–529.

26. El-Deiry, W.S., Winer, A., Slifker, M., Taylor, S., Adamson, B.J.S., Meropol, N.J., and Ross, E.A. (2019). Disease control with FOLFIRI plus ziv-aflibercept (zFOLFIRI) beyond FOLFIRI plus bevacizumab: case series in metastatic colorectal cancer (mCRC). Front. Oncol. *9*, 142.

27. Dey, N., De, P., and Brian, L.J. (2015). Evading anti-angiogenic therapy: resistance to anti-angiogenic therapy in solid tumors. Am. J. Transl. Res. *7*, 1675–1698.

28. Kurihara, R., Yamaoka, K., Sawamukai, N., Shimajiri, S., Oshita, K., Yukawa, S., Tokunaga, M., Iwata, S., Saito, K., Chiba, K., et al. (2010). C5a promotes migration, proliferation, and vessel formation in endothelial cells. Inflamm. Res. *59*, 659–666.

29. Klein, R.J., Zeiss, C., Chew, E.Y., Tsai, J.Y., Sackler, R.S., Haynes, C., Henning, A.K., SanGiovanni, J.P., Mane, S.M., Mayne, S.T., et al. (2005). Complement factor H polymorphism in age-related macular degeneration. Science *308*, 385–389.

30. Li, Y., Zhu, P., Verma, A., Prasad, T., Deng, H., Yu, D., and Li, Q. (2017). A novel bispecific molecule delivered by recombinant AAV2 suppresses ocular inflammation and choroidal neovascularization. J. Cell. Mol. Med. *21*, 1555–1571.

31. Pio, R., Ajona, D., and Lambris, J.D. (2013). Complement inhibition in cancer therapy. Semin. Immunol. *25*, 54–64.

32. Markiewski, M.M., and Lambris, J.D. (2009). Is complement good or bad for cancer patients? A new perspective on an old dilemma. Trends Immunol. *30*, 286–292.

33. Oner, F., Savas, I., and Numanoglu, N. (2004). Immunoglobulins and complement components in patients with lung cancer. Tuberk. Toraks. *52*, 19–23.

34. Ytting, H., Jensenius, J.C., Christensen, I.J., Thiel, S., and Nielsen, H.J. (2004). Increased activity of the mannan-binding lectin complement activation pathway in patients with colorectal cancer. Scand. J. Gastroenterol. *39*, 674–679.

35. Bjørge, L., Hakulinen, J., Vintermyr, O.K., Jarva, H., Jensen, T.S., Iversen, O.E., and Meri, S. (2005). Ascitic complement system in ovarian cancer. Br. J. Cancer *92*, 895–905.

36. Riihilä, P., Nissinen, L., Farshchian, M., Kallajoki, M., Kivisaari, A., Meri, S., Grénman, R., Peltonen, S., Peltonen, J., Pihlajaniemi, T., et al. (2017). Complement component C3 and complement factor B promote growth of cutaneous squamous cell carcinoma. Am. J. Pathol. *187*, 1186–1197.

37. Zhao, C., Li, Y., Qiu, W., He, F., Zhang, W., Zhao, D., Zhang, Z., Zhang, E., Ma, P., Liu, Y., et al. (2018). C5a induces A549 cell proliferation of non-small cell lung cancer via GDF15 gene activation mediated by GCN5-dependent KLF5 acetylation. Oncogene *37*, 4821–4837.

38. Mollnes, T.E., and Kirschfink, M. (2006). Strategies of therapeutic complement inhibition. Mol. Immunol. *43*, 107–121.

39. Bondar, T., and Medzhitov, R. (2013). The origins of tumor-promoting inflammation. Cancer Cell *24*, 143–144.

40. Valencia, T., Kim, J.Y., Abu-Baker, S., Moscat-Pardos, J., Ahn, C.S., Reina-Campos, M., Duran, A., Castilla, E.A., Metallo, C.M., Diaz-Meco, M.T., and Moscat, J. (2014). Metabolic reprogramming of stromal fibroblasts through p62-mTORC1 signaling promotes inflammation and tumorigenesis. Cancer Cell *26*, 121–135.

41. Dai, L., Cui, X., Zhang, X., Cheng, L., Liu, Y., Yang, Y., Fan, P., Wang, Q., Lin, Y., Zhang, J., et al. (2016). SARI inhibits angiogenesis and tumour growth of human colon cancer through directly targeting ceruloplasmin. Nat. Commun. *7*, 11996.

42. Ostrand-Rosenberg, S. (2008). Cancer and complement. Nat. Biotechnol. *26*, 1348–1349.

43. Ning, C., Li, Y.Y., Wang, Y., Han, G.C., Wang, R.X., Xiao, H., Li, X.Y., Hou, C.M., Ma, Y.F., Sheng, D.S., et al. (2015). Complement activation promotes colitis-associated carcinogenesis through activating intestinal IL-1β/IL-17A axis. Mucosal Immunol. *8*, 1275–1284.

44. Horikawa, N., Abiko, K., Matsumura, N., Hamanishi, J., Baba, T., Yamaguchi, K., Yoshioka, Y., Koshiyama, M., and Konishi, I. (2017). Expression of vascular endothelial growth factor in ovarian cancer inhibits tumor immunity through the accumulation of myeloid-derived suppressor cells. Clin. Cancer Res. *23*, 587–599.

45. Ebos, J.M., and Kerbel, R.S. (2011). Antiangiogenic therapy: impact on invasion, disease progression, and metastasis. Nat. Rev. Clin. Oncol. *8*, 210–221.

46. Motallebnezhad, M., Jadidi-Niaragh, F., Qamsari, E.S., Bagheri, S., Gharibi, T., and Yousefi, M. (2016). The immunobiology of myeloid-derived suppressor cells in cancer. Tumour Biol. *37*, 1387–1406.

47. Umansky, V., Blattner, C., Gebhardt, C., and Utikal, J. (2016). The role of myeloid-derived suppressor cells (MDSC) in cancer progression. Vaccines (Basel) *4*, E36.

48. Kochanek, D.M., Ghouse, S.M., Karbowniczek, M.M., and Markiewski, M.M. (2018). Complementing cancer metastasis. Front. Immunol. *9*, 1629.

49. Hu, W.H., Hu, Z., Shen, X., Dong, L.Y., Zhou, W.Z., and Yu, X.X. (2016). C5a receptor enhances hepatocellular carcinoma cell invasiveness via activating ERK1/2-mediated epithelial-mesenchymal transition. Exp. Mol. Pathol. *100*, 101–108.

50. Condamine, T., Ramachandran, I., Youn, J.I., and Gabrilovich, D.I. (2015). Regulation of tumor metastasis by myeloid-derived suppressor cells. Annu. Rev. Med. *66*, 97–110.

51. Pulaski, B.A., and Ostrand-Rosenberg, S. (2001). Mouse 4T1 breast tumor model. Curr. Protoc. Immunol. *39*, 20.2.1–20.2.16.

OMTO, Volume *16*

Supplemental Information

A Novel Antitumor Strategy: Simultaneously Inhibiting Angiogenesis and Complement by Targeting VEGFA/PlGF and C3b/C4b

Huiling Wang, Yiming Li, Gang Shi, Yuan Wang, Yi Lin, Qin Wang, Yujing Zhang, Qianmei Yang, Lei Dai, Lin Cheng, Xiaolan Su, Yang Yang, Shuang Zhang, Zhi Li, Jia Li, Yuquan Wei, Dechao Yu, and Hongxin Deng

Supplemental Figures

Figure S1

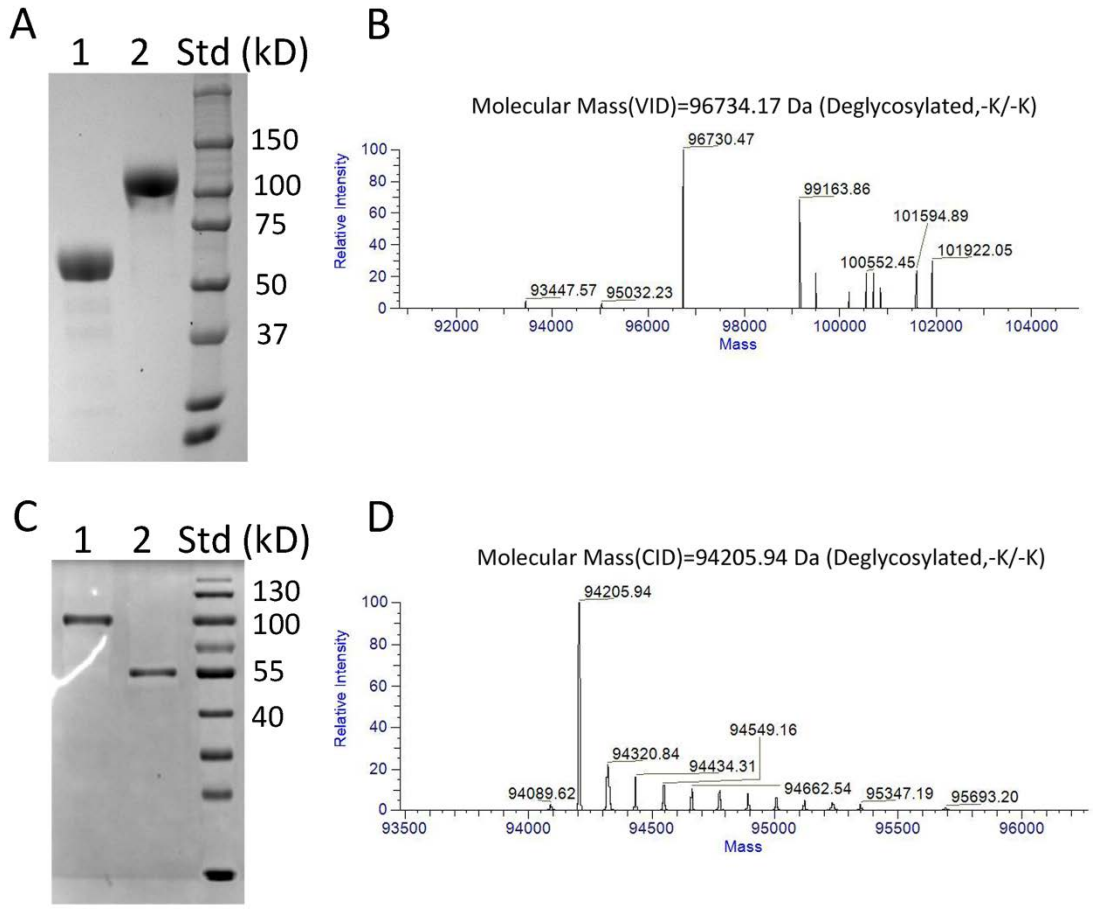

Figure S1: Molecular Characteristics of VID and CID. (A) The molecular mass of dimer/monomer VID analyzed by SDS-PAGE. Lane 1, the monomer form of VID; lane 2, the dimer form of VID; right, positions of molecular weight markers in kilodaltons (kDa). (B) Molecular weight of deglycosylated VID by HPLC-MS. (C) The molecular mass of dimer/monomer CID analyzed by SDS-PAGE. Lane 1, the CID dimer form of; lane 2, the monomer form of CID; right, positions of molecular weight markers in kilodaltons (kDa). (D) Molecular weight of deglycosylated CID by HPLC-MS.

Figure S2

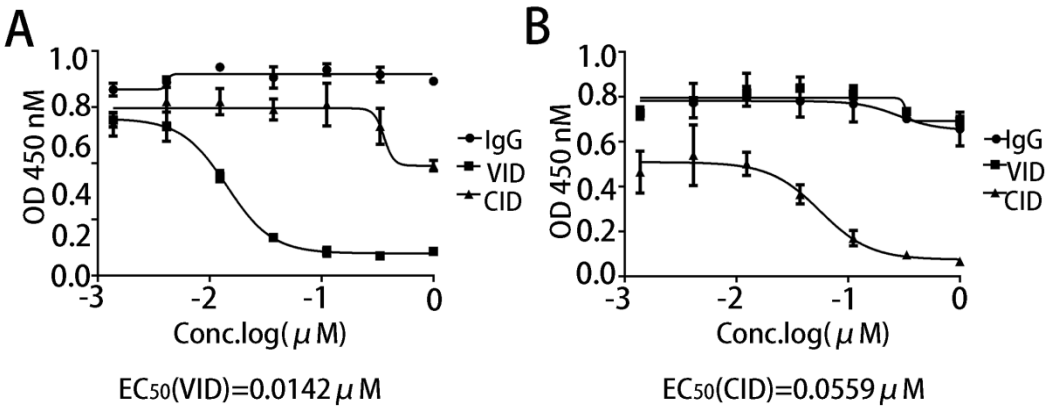

Figure S2: The competitive binding assays of VID and CID. The coated antigen and competitive antigen are different. (A) KDR and VID/CID/IgG are allowed to compete for binding with biotinylated VEGF165. The error bars represent SD. (B) CD35 and VID/CID/IgG are allowed to compete for binding with biotinylated C4b. The error bars represent SD.

Figure S3

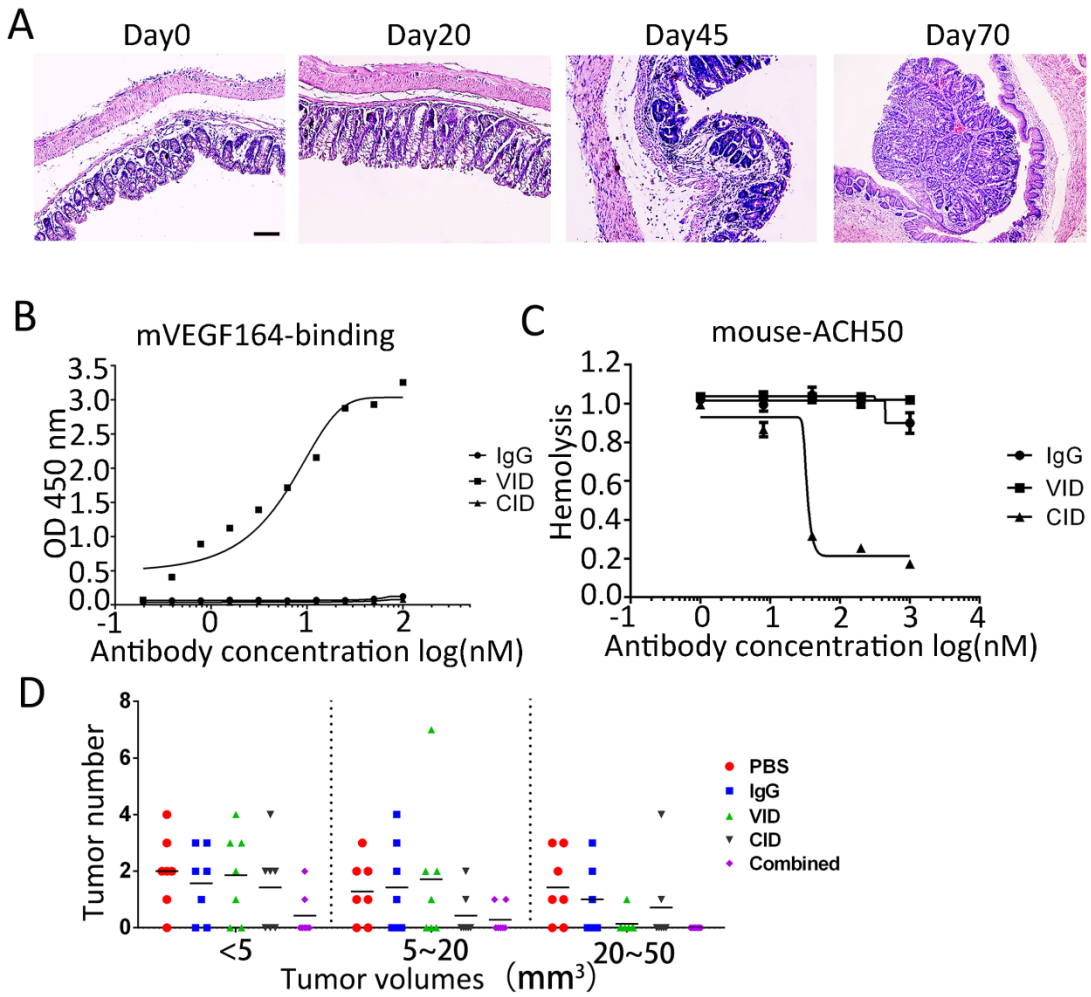

Figure S3: Complement activation in azoxymethane/dextran sulfate sodium (AOM/DSS)-induced colitis-associated cancer. (A) H&E stain validation model establishment. Original magnifications 100×, Scale bar = 50 μ m. (B) Bindings of VID to mouse-VEGF164 as determined by ELISA with bars representing SD. (C) CID inhibits the activation of mouse-ACH50. The error bars represent SD. (D) The number of tumors in different volume groups was compared.

Figure S4

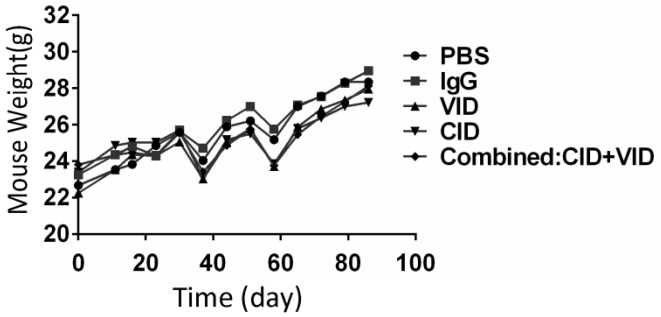

Figure S4: Body weight of mice in each group was measured on the days indicated. The error bars represent SD.

Figure S5

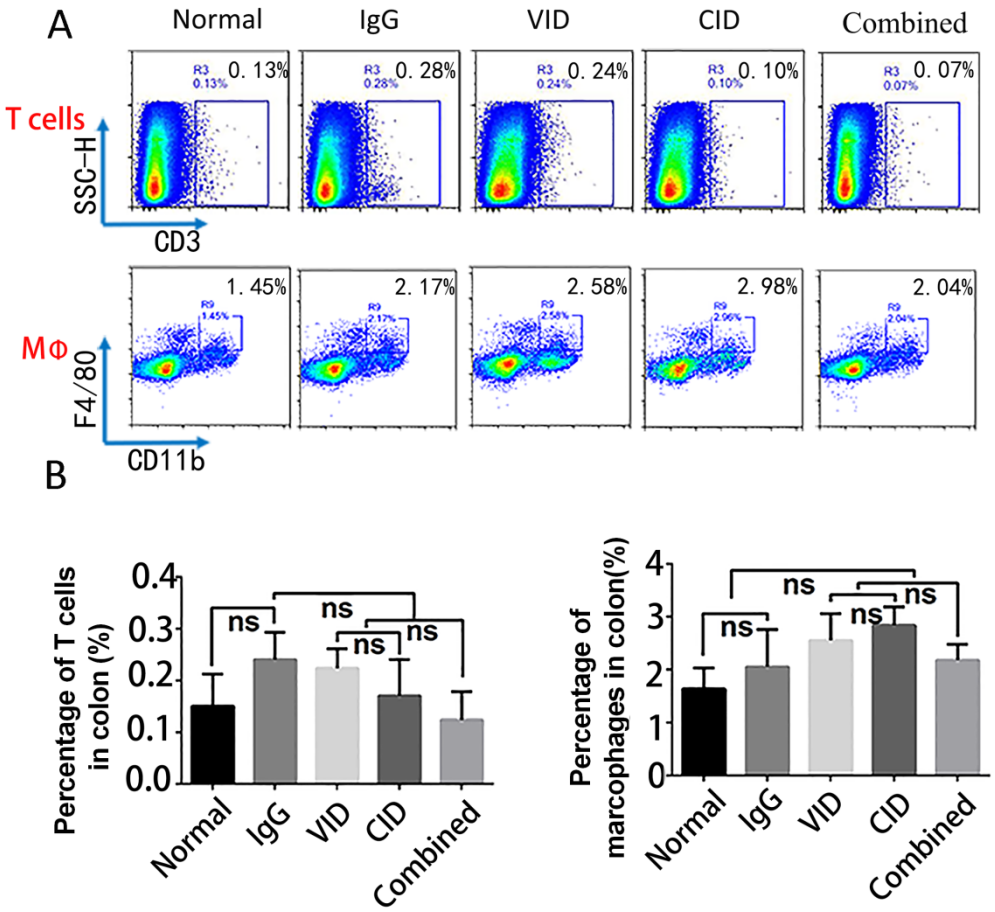

Figure S5: Infiltration of T cells and Macrophage in colon. (A) Infiltration of T cells and Macrophage in colon was analyzed by flow cytometry. (B) Quantification

analyses of T cells (CD3 positive cells) and Macrophage (F4/80+CD11b positive cells) numbers in colon (ns means not significant). The error bars represent SD.

Figure S6

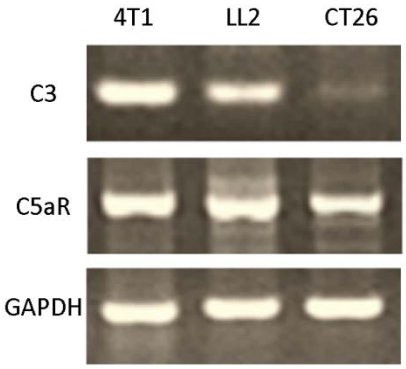

Figure S6: RT-PCR results showed C3 and C5aR transcription levels in 4T1, LL/2, CT26 cell lines.

Figure S7

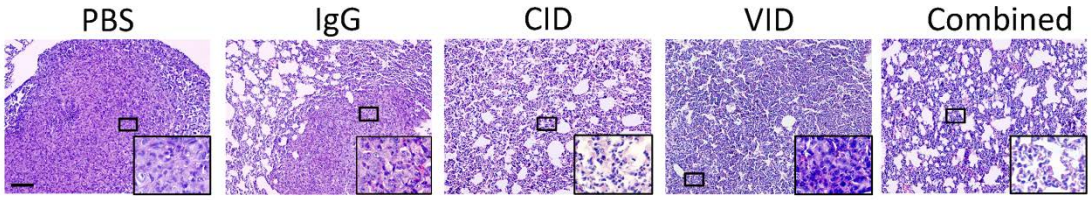

Figure S7: Lung metastases of 4T1 cells in different groups. H&E-stained sections of the lungs of each group. Original magnifications 200×, Scale bar = 50μm.